ANNALS OF THE CHRYSENE FORMALISM
RESEARCH ARTICLE | AI-AUGMENTED PEER REVIEWED | VOL. 1, NO. 1 | SEPTEMBER 2026

# Redox-Controlled Functional Differentiation of Dual-Chrysene Catalyst Families: The Hopane–Sterane Record across the GOE and NOE

**Charles D. Schaper, Ph.D.**
*Chief Editor, Annals of the Chrysene Formalism*
*San Francisco, California, USA*
editor@chrysene.com

## Abstract

The contamination-controlled molecular fossil record exhibits a pronounced temporal asymmetry: hopanes dominate mid-Proterozoic assemblages while remaining abundant, and regular 4-desmethyl steranes rise only from the late Tonian onward. Independent paleoredox proxies partition the same interval into three successive atmospheric regimes—primordial anaerobic conditions ($pO_2 < 10^{-5}$ PAL), post-GOE mid-Proterozoic conditions ($\sim$ 0.1–2 % PAL), and the Neoproterozoic rise toward modern levels ($\sim$ 21 % absolute). Under the Identification Hypothesis the dual-chrysene reactive volume of U.S. Patent 12,195,423 supplies both Family H (hopanoid-directed) and Family S (sterol-directed) geometries under anaerobic conditions. Family H is constitutively processed into membrane-embedded hopanoids. Family S is initially present at low concentration as a gene- and membrane-associated complex; a structural correspondence between the sterane-family substitution pattern and nucleobase-pairing loci supplies a geometric basis for possible intercalation. As the redox parameter $\rho$ rises, the concentration of Family S increases and the geometry undergoes a continuous transition into a cholesterol-like membrane component that contributes to membrane fluidity, stability and signalling. Both families begin as exogenous products of the metamaterial and are later captured endogenously. The mid-Proterozoic hopane dominance and late-Tonian sterane rise, occurring against persistent hopane abundance, are the geological expression of this redox-controlled functional differentiation. The underlying lattice, the $C_{2h}$ symmetry of each core, and the chiral step-defect remain invariant.

**Keywords:** dual-chrysene reactive volume; Family H catalysts; Family S catalysts; intercalation; membrane–gene coupling; cholesterol; hopane/sterane asymmetry; Great Oxidation Event; Neoproterozoic Oxygenation Event; Patent US 12,195,423; Identification Hypothesis; chiral step-defect

# 1 Introduction

## 1.1 Empirical Problem Statement

Let $\mathcal{R}$ denote the contamination-controlled molecular fossil record of marine sedimentary organic matter, and let $\mathcal{P}$ denote the independent paleoredox proxy record (S-MIF, Ce anomalies, Cr isotopes, Mo–U enrichment, Fe speciation, and related indicators). Within the joint data set $(\mathcal{R}, \mathcal{P})$ the following regularities are established.

1. In mid-Proterozoic successions the extractable and kerogen-bound hydrocarbon assemblages are dominated by hopanes, with sterane/hopane ratios satisfying $S/H \ll 1$. Absolute hopane abundances remain significant; the scarcity of steranes is not accompanied by a collapse of the hopane signal.

2. Regular 4-desmethyl steranes become detectable and ecologically significant only in the late Tonian (approximately 820–720 Ma). Thereafter $S/H$ rises by one to two orders of magnitude while hopanes continue to be recovered in substantial quantities.

3. The oldest secure geoporphyrin assemblages (Taoudeni Basin, $\sim$ 1.1 Ga) occupy the carbon-number window $C_{28}$–$C_{34}$, occur as Ni or VO complexes, and retain an 18 $\pi$-electron aromatic core.

4. Independent paleoredox proxies partition Earth history into three successive atmospheric regimes:

   - Window 0: primordial–Archean anaerobic conditions ($pO_2 < 10^{-5}$ PAL);
   - Window 1: post-GOE to mid-Proterozoic conditions

**Citation:** Schaper, C. D. (2026). Redox-Controlled Functional Differentiation of Dual-Chrysene Catalyst Families: The Hopane–Sterane Record across the GOE and NOE. *Annals of the Chrysene Formalism*, 1(1), 259–272. https://chrysene.com/index.php/acf/article/view/22  First published by Schaper Systems Press in the *Annals of the Chrysene Formalism*, Vol. 1, No. 1 (2026).

(∼ 0.1–2 % PAL);

- Window 2: Neoproterozoic Oxygenation Event and subsequent rise toward modern levels (∼ 21 % absolute).

These observations raise a precise geometric question: does there exist a single, persistent structural feature that is already competent under the anaerobic conditions of Window 0, that accounts for the continued abundance of hopanoids alongside the later rise of steranes, and that is consistent with the co-occurrence of the chrysene-family skeleton and the redox-sensitive geoporphyrin record?

### 1.2 Chrysene Formalism Prediction and the Identification Hypothesis

Under the Identification Hypothesis the pure-mathematical manifold $I_C$ is realized by the physical chrysene lattice of U.S. Patent 12,195,423. A dual-chrysene reactive volume consists of two tetrasubstituted chrysene units of native $C_{2h}$ symmetry that jointly define a base-four configuration. One unit occupies the substrate position and is transformed, under the nitridation and anaerobic-oxidation conditions of the patent, into a nucleobase pair; the second unit occupies the catalyst position.

Two disjoint families of catalyst geometries are distinguished:

- Family H (hopanoid-directed), drawn from the $3, 6, 9, 12$-substitution class;
- Family S (sterol-directed), drawn from the $2, 5, 8, 11$-substitution class.

Both families are generated by the reactive volume already under anaerobic conditions. The patent further records a structural correspondence between the sterane-family substitution pattern (particularly at the loci that become the $2, 5, 8, 11$ positions) and the geometry of nucleobase pairing. This correspondence supplies a geometric basis for intercalation of Family-S molecules into nascent nucleic-acid frameworks.

### 1.3 1.3. Central Claim

**Claim 1.** *The dual-chrysene reactive volume of U.S. Patent 12,195,423 generates both Family H and Family S geometries under the anaerobic conditions of Window 0. Family H is constitutively converted into membrane-embedded hopanoids. Family S is initially present at low concentration as a gene- and membrane-associated complex; a structural correspondence recorded in the patent between the sterane-family substitution pattern and nucleobase-pairing loci supplies a geometric basis for possible intercalation. As $\rho$ rises, the concentration of Family S increases and the geometry undergoes a continuous transition into a cholesterol-like membrane component that contributes to membrane fluidity, stability and signalling. Both families begin as exogenous products of the metamaterial and are later captured endogenously. The mid-Proterozoic hopane dominance and late-Tonian sterane rise, occurring against persistent hopane abundance, are the geological expression of this redox-controlled functional differentiation. The lattice, $C_{2h}$ symmetry, and chiral step-defect remain invariant.*

### 1.4 Roadmap

The argument proceeds in four stages.

1. The empirical boundary conditions furnished by the hopane/sterane record, the geoporphyrin archive, and the independent paleoredox proxies are fixed without theoretical interpretation (Section 2).
2. The dual-chrysene volume is formalized, the two functional states of Family S are defined, the silencing-efficacy and concentration functions are introduced, and the membrane–gene mapping is stated as a geometric consequence of the $\Sigma \to \mathrm{M}$ transition (Section 3).
3. These geometric predictions are confronted with the observational constraints across the three oxygen windows, with explicit attention to the persistence of hopanes alongside the rise of steranes.
4. A set of concrete, testable consequences and open experimental targets is recorded.

## 2 Empirical Framework – Data Constraints

The geometric constructions of subsequent sections are required to be consistent with the following observational boundary conditions. No theoretical interpretation is advanced in the present section; the data are recorded solely as empirical constraints that any successful geometric account must recover.

### 2.1 The Three Atmospheric Oxygen Windows

**Definition 1** (Normalized Redox Parameter)**.** *Let $\rho \in [0, 1]$ be the normalized environmental oxygen fugacity. The unit interval is partitioned into three successive windows corresponding to the principal secular regimes of atmospheric oxygenation:*

1. ***Window 0*** *($\rho = 0$): the primordial–Archean anaerobic regime ($p\mathrm{O}_2 < 10^{-5}$ PAL), realized approximately on the interval* 4.0–2.4 Ga.
2. ***Window 1*** *($0 < \rho \lesssim 10^{-2}$): the post-GOE to mid-Proterozoic regime, commencing with the Great Oxi-*

*dation Event (onset* $\sim$ 2.46–2.42 Ga*, irreversible rise by* $\sim$ 2.33–2.22 Ga*) and persisting through the "Boring Billion" (*$\sim$ 1.8–0.8 Ga*), with atmospheric oxygen stabilized near* 0.1–2 % *PAL.*

3. ***Window 2*** *(*$\rho \gtrsim \rho_*$*): the Neoproterozoic Oxygenation Event and subsequent regime (*$\sim$ 0.85–0.54 Ga *onward), during which* $pO_2$ *rises toward modern levels (*$\sim$ 21 % *absolute).*

**Remark 1.** *The numerical bounds on* $\rho$ *are conventional normalizations chosen for notational convenience; the essential empirical content is the existence of three qualitatively distinct redox regimes whose temporal boundaries are fixed by independent geochemical proxies (disappearance of mass-independent sulfur-isotope fractionation, appearance of terrestrial red beds, cerium anomalies, chromium isotopes, and related indicators).*

## 2.2 Hopane–Sterane Record

**Proposition 1** (Mid-Proterozoic Hopane Dominance)**.** *In Paleoproterozoic and Mesoproterozoic successions examined under rigorous contamination-control protocols, hopanes constitute the dominant polycyclic terpenoid class recovered from both the extractable bitumen and the kerogen-bound fractions. The sterane/hopane ratio satisfies*

$$S/H \ll 1$$

*and is frequently indistinguishable from analytical blank levels. Extended hopanes (*$C_{31}$–$C_{35}$*) are routinely present. Absolute hopane abundances remain significant; the scarcity of steranes is not accompanied by a collapse of the hopane signal.*

**Proposition 2** (Late-Tonian Sterane Rise with Persistent Hopanes)**.** *Regular* 4*-desmethyl steranes (cholestane* $C_{27}$*, ergostane* $C_{28}$*, stigmastane* $C_{29}$*) remain below reliable detection limits, or yield*

$$S/H \leq 10^{-3},$$

*in the great majority of mid-Proterozoic samples. A sustained rise in abundance and diversity begins in the late Tonian, with first consistent appearances between approximately* 820 *and* 720 Ma*. Thereafter* $S/H$ *ratios increase by one to two orders of magnitude. Critically, hopanes continue to be recovered in substantial quantities; the rise in the ratio is driven primarily by the addition and ecological expansion of the sterane signal rather than by a wholesale decline in hopane abundance.*

**Proposition 3** (Continuity into the Phanerozoic)**.** *Both hopanoid and sterol biosynthetic pathways remain active in the modern biosphere. Hopanoids continue to be produced by diverse bacterial lineages; sterols (including cholesterol) are universal components of eukaryotic membranes.*

## 2.3 Geoporphyrin Record

**Proposition 4** (1.1 Ga Taoudeni Basin Assemblage)**.** *The oldest secure molecular record of chlorophyll-derived pigments consists of intact nickel and vanadyl geoporphyrins recovered from marine black shales of the Taoudeni Basin (Mauritania), dated at approximately* 1.1 Ga*. The dominant species occupy the carbon-number interval* $C_{28}$–$C_{34}$ *and belong predominantly to the deoxophylloerythroetioporphyrin (DPEP) and etioporphyrin (Etio) structural classes. The porphyrins occur almost exclusively as nickel(II) or vanadyl (*$VO^{2+}$*) complexes. Nitrogen-isotope values are consistent with a predominantly cyanobacterial source. This assemblage lies firmly inside the hopane-dominated regime of Window 1.*

**Proposition 5** (Maturity and Metal Trends)**.** *Across the wider sedimentary record the following regularities are repeatedly observed:*

1. *With increasing thermal maturity the relative abundance of DPEP declines while that of Etio rises.*
2. *The long isoprenoid (phytol) side-chain of biological chlorophyll is absent from all but the most immature assemblages; only the metal-coordinated tetrapyrrole core, together with short alkyl substituents, survives.*
3. *Regardless of maturity or metal identity, the preserved molecules retain a fully conjugated tetrapyrrole macrocycle whose aromatic pathway comprises eighteen* $\pi$*-electrons.*

## 2.4 Independent Paleoredox Proxies

**Proposition 6** (Proxy Constraints on the Three Windows)**.** *The temporal boundaries and approximate oxygen levels of the three windows of Definition 1 are independently constrained by the following classes of paleoredox indicators (among others):*

1. *Mass-independent fractionation of sulfur isotopes (S-MIF), which disappears once* $pO_2$ *exceeds* $\sim 10^{-5}$ *PAL and thereby marks the irreversible onset of the GOE.*
2. *Cerium anomalies, chromium isotopes, and related redox-sensitive elemental ratios that constrain mid-*

*Proterozoic $pO_2$ to the approximate range* 0.1–2 % *PAL.*

3. *Molybdenum and uranium enrichment patterns, iron speciation, and sulfate-isotope systematics that record the progressive oxygenation of the oceans during the Neoproterozoic.*

*Collectively these proxies fix the stratigraphic intervals that correspond to Windows 0, 1 and 2 without reference to the hopane/sterane or geoporphyrin records.*

### 2.5 Scope Limitation

**Proposition 7** (Boundary Conditions Only)**.** *The mapping of the chrysene step-defect onto paired nucleobases is taken as already established by U.S. Patent 12,195,423 and is cited only; no new conformational analysis of DNA or RNA is undertaken. The empirical constraints assembled above—the three oxygen windows, the hopane/sterane asymmetry with persistent hopanes, the geoporphyrin carbon-number and metal patterns, and the independent paleoredox proxies—are fixed before any geometric model is introduced. All subsequent constructions are required to be consistent with these data; they are not derived from them.*

**Remark 2.** *The patent conditions themselves constitute an empirical boundary condition of Window 0: the dual-chrysene processes of U.S. Patent 12,195,423 are demonstrated under anaerobic conditions and thereby establish the competence of the metamaterial at $\rho = 0$. This competence is recorded here solely as an observational fact; its geometric interpretation is deferred to Section 3.*

## 3 Geometric Model of Co-existence, Silencing, and Membrane–Gene Coupling

Throughout this section the Identification Hypothesis is assumed. All constructions are understood as images under the structure-preserving map

$$\Phi : I_C \longrightarrow \mathcal{M},$$

where $I_C$ denotes the pure-mathematical Chrysene Tensor Space and $\mathcal{M}$ the category of molecular graphs equipped with $\pi$-electron counts, coordination data, intercalation competence and redox-dependent kinetic measures.

### 3.1 Dual Presence under Anaerobic Conditions

**Definition 2** (Dual-Chrysene Reactive Volume)**.** *A* dual-chrysene reactive volume *is a base-four configuration formed by the non-commutative spatial orientation of exactly two substituted chrysene cores of native $C_{2h}$ symmetry. One core occupies the substrate position and is transformed, under the nitridation and anaerobic-oxidation conditions of U.S. Patent 12,195,423, into a nucleobase pair. The second core occupies the catalyst position. The volume simultaneously generates members of both catalyst families defined below.*

**Definition 3** (Catalyst Families)**.**

- ***Family H*** *(hopanoid-directed): geometries belonging to the* $3, 6, 9, 12$*-substitution class, preferentially the* $6, 12$*- and* $3, 6, 12$*-patterns.*
- ***Family S*** *(sterol-directed): geometries belonging to the* $2, 5, 8, 11$*-substitution class.*

*Both families are present in the reactive volume already at $\rho = 0$.*

**Proposition 8** (Constitutive Membrane Embedding of Family H)**.** *Under anaerobic conditions Family H is rapidly converted into hopanoid-class polycycles that are constitutively integrated into the membrane lipid fraction. The process is essentially irreversible on geological time-scales and remains largely independent of subsequent increases in $\rho$.*

### 3.2 Dual Functional States of Family S

**Definition 4** (Functional States of Family S)**.** *Family S (the* $2, 5, 8, 11$*-substituted geometry) admits at least two geometrically admissible readings:*

1. *a membrane-associated reading in which the geometry contributes to membrane fluidity, stability and signalling;*
2. *an intercalation-competent reading in which the structural correspondence recorded in U.S. Patent 12,195,423 between the sterane-family substitution pattern and nucleobase-pairing loci permits intercalation into nucleic-acid frameworks.*

*Neither reading is required by the concentration dynamics or by the explanation of the hopane–sterane record; both remain open geometric possibilities.*

**Definition 5** (Patent Structural Correspondence)**.** *U.S. Patent 12,195,423 records a structural correspondence between the sterane-family substitution pattern (particularly at the loci that become the* $2, 5, 8, 11$ *positions) and the geometry of nucleobase pairing. This correspondence supplies a geometric basis for intercalation of Family-S molecules into nucleic-acid duplexes, thereby enabling the silencing function of State* $\Sigma$ *while endogenous regulatory circuitry remains incomplete.*

**Definition 6** (Silencing Efficacy)**.** *Let* $\sigma(\rho) \in [0, 1]$ *be a monotonically decreasing smooth function of the redox parameter that quantifies the residual silencing efficacy of Family S. By definition*

$$\sigma(0) = 1, \qquad \lim_{\rho \to 1} \sigma(\rho) = 0.$$

**Definition 7** (Concentration of Family S)**.** *Let* $c_S(\rho)$ *denote the effective concentration (or occupancy measure) of Family-S geometries. It is a monotonically increasing smooth function of* $\rho$ *satisfying*

$$c_S(0) \ll 1, \qquad \lim_{\rho \to 1} c_S(\rho) = c_S^{\max}.$$

**Proposition 9** (Redox-Controlled Functional Transition)**.** *The instantaneous silencing activity of Family S is measured by the product* $\sigma(\rho)\, c_S(\rho)$*. As* $\rho$ *rises,* $\sigma(\rho)$ *declines while* $c_S(\rho)$ *increases. The net effect is a progressive release from silencing accompanied by a rise in the structural (State* M*) population.*

## 3.3 Membrane–Gene Mapping and Signaling

**Definition 8** (Membrane–Gene Correspondence)**.** *If the silencing reading (State* $\Sigma$*) is active, the continuous transition* $\Sigma \to \mathrm{M}$ *induces a geometric correspondence between the membrane-embedded sterol component and the gene loci previously occupied by intercalation. The shared substitution pattern that mediated intercalation becomes, after the transition, a structural link associating the membrane component with those loci. The resulting map*

$$\Phi_{\Sigma \to \mathrm{M}} : \begin{array}{c} \textit{membrane component of State } \mathrm{M} \\ \longrightarrow \\ \textit{previously intercalated gene loci} \end{array}$$

*is well-defined as a formal geometric object. Its interpretation as a functional redox-sensitive signalling channel is optional and is not required by the algebraic concentration dynamics.*

**Proposition 10** (Signaling Competence)**.** *Once the membrane–gene mapping* $\Phi_{\Sigma \to \mathrm{M}}$ *of Definition 8 is realized, changes in external oxygen fugacity are transducible into differential regulatory states at the previously silenced loci. Because the membrane component remains geometrically associated with the loci it once occupied by intercalation, modulation of membrane composition or physical state by rising* $\rho$ *can be read as a regulatory signal at those sites. The mapping therefore converts a purely geometric intercalation competence into a functional, redox-dependent signaling mechanism.*

**Proposition 11** (Optional Signalling Reading)**.** *When the map* $\Phi_{\Sigma \to \mathrm{M}}$ *is given the signalling interpretation, changes in external oxygen fugacity become transducible into differential states at the previously intercalated loci. This reading converts intercalation competence into a possible signalling mechanism; it is not a necessary consequence of the operators.*

**Definition 9** (Release, Replication, and Quantitative Expansion)**.** *Full release from intercalation (*$\sigma(\rho) \to 0$*) removes the steric and energetic barrier that had restrained replication at the previously silenced loci. Unimpeded cellular replication can then proceed. Thereafter the membrane-bound population in State* M *expands quantitatively with eukaryotic abundance, producing a secular rise in the sterane signal while the hopanoid inventory supplied by Family H remains substantial.*

## 3.4 Exogenous Supply and Endogenous Capture

**Definition 10** (Exogenous-to-Endogenous Transition)**.** *Both Family H and Family S are initially supplied exogenously by the dual-chrysene metamaterial. Subsequent evolutionary capture by the squalene-cyclase / oxidosqualene-cyclase superfamily and associated tailoring enzymes converts each geometry into an endogenous biosynthetic pathway, thereby eliminating obligatory dependence on external supply of the substituted chrysene cores while preserving the functional distinction between the two families.*

### 3.5 Invariance of the Geometric Core

**Theorem 12** (Redox Invariance of the Lattice)**.** *The underlying dual-chrysene lattice, the $C_{2h}$ symmetry of each core, the four-arm coordination geometry, and the chiral step-defect are independent of the parameter $\rho$. The geometric core remains invariant independently of which functional reading—membrane-only or intercalation-competent—is assigned to Family S.*

*Proof.* The structure-preserving map $\Phi$ factors through the combinatorial graph of the chrysene lattice. The redox parameter enters solely through the silencing-efficacy and concentration functions of Definitions 6 and 7 and through the mapping of Definition 8; it leaves the geometric objects themselves unaltered. □

**Corollary 1** (Persistence of the Step-Defect)**.** *The chiral step-defect fixed under the anaerobic conditions of the patent is transmitted unaltered into both the hopanoid products of Family H and the cholesterol-like products of Family S (State* M*).*

### 3.6 Three-Phase Geometric Timeline

**Definition 11** (Three-Phase Partition under Co-existence)**.**

1. ***Phase 0*** *($\rho = 0$): both families present; Family H rapidly membrane-embedded as hopanoids; Family S present at low concentration in State $\Sigma$ (silencing).*
2. ***Phase I*** *(Window 1): Family H continues to dominate the membrane lipid inventory; Family S remains primarily regulatory ($\sigma(\rho)$ still significant, $c_S(\rho)$ still low), producing only trace sterane signals.*
3. ***Phase II*** *(Window 2): $\sigma(\rho)$ declines and $c_S(\rho)$ rises; the $\Sigma \to$ M transition is realized, the membrane–gene mapping becomes active, silencing is released, and the membrane-bound sterane population expands quantitatively with eukaryotic abundance, generating the observed late-Tonian rise of regular steranes while hopanes remain abundant.*

**Theorem 13** (Geometric Origin of the Stratigraphic Pattern)**.** *The mid-Proterozoic hopane dominance and the late-Tonian sterane rise, occurring against a background of persistent hopane abundance, are the geological expression of the redox-controlled functional differentiation of co-existing Family H and Family S geometries. The differentiation begins from the anaerobic exogenous supply of the dual-chrysene volume, proceeds through silencing and membrane–gene coupling, and culminates in the endogenous production of both hopanoids and cholesterol-like sterols together with the quantitative expansion of the sterane signal.*

## 4 Confrontation with Observational Constraints

The geometric constructions of Section 3 are now confronted with the empirical boundary conditions of Section 2. The confrontation is organized by the three oxygen windows of Definition 1. No additional hypotheses are introduced; each statement records a direct consistency between a geometric prediction and an observational regularity already fixed.

### 4.1 Window 0: Anaerobic Co-existence

**Proposition 14** (Consistency at $\rho = 0$)**.** *Under the anaerobic conditions of Window 0 both families are present (Definition 3). Family H is constitutively converted into membrane-embedded hopanoids (Proposition 8). Family S occupies State $\Sigma$ at low concentration, with intercalation competence supplied by the patent structural correspondence (Definitions 4 and 5). This configuration is consistent with the empirical competence of U.S. Patent 12,195,423 under nitridation and anaerobic-oxidation conditions.*

**Remark 3.** *Window 0 supplies the absolute geometric baseline. All subsequent redox evolution is measured relative to this anaerobic ground state of co-existence.*

### 4.2 Window 1: Persistent Hopane Dominance and Regulatory Family S

**Proposition 15** (Hopane Dominance in Window 1)**.** *Throughout Window 1 the membrane lipid inventory remains dominated by the hopanoid products of Family H, while Family S continues to reside primarily in the regulatory regime of low $c_S(\rho)$ and significant $\sigma(\rho)$. Consequently the extractable and kerogen-bound polycyclic inventory is predicted to satisfy*

$$S/H \ll 1$$

*with absolute hopane abundances remaining substantial. This prediction recovers the contamination-controlled mid-Proterozoic record of Proposition 1, including the* 1.1 Ga *Taoudeni Basin interval.*

**Proposition 16** (Geoporphyrin Preferences in Window 1)**.** *The same low-$\rho$ regime is compatible with nickel coordination and retention of the DPEP structural class. The*

*observed predominance of Ni-DPEP assemblages at* 1.1 Ga *(Proposition 4) lies inside the geometric envelope fixed by Window 1.*

### 4.3 Window 2: Release from Silencing and Sterane Expansion

**Proposition 17** (Sterane Rise with Persistent Hopanes in Window 2)**.** *Once $\rho$ enters Window 2 the* $\Sigma \to$ M *transition and membrane–gene mapping of Definitions 8–9 are realized. Silencing is released, cellular replication proceeds, and the membrane-bound population in State* M *expands quantitatively with eukaryotic abundance. Family H continues to supply hopanoids. The net geological signature is a rise in $S/H$ by one to two orders of magnitude against a background of persistent hopane abundance—precisely the pattern recorded in Proposition 2.*

**Proposition 18** (Geoporphyrin Evolution in Window 2)**.** *The same rise in $\rho$ is compatible with an increased relative abundance of vanadyl complexes and with the maturity-driven conversion of DPEP to Etio (Proposition 5).*

### 4.4 Multi-Archive Coherence

**Theorem 19** (Simultaneous Consistency)**.** *The dual-chrysene volume, operating through the co-existence and functional differentiation formalized in Section 3, accounts simultaneously for:*

1. *the hopane-dominated mid-Proterozoic assemblages and the late-Tonian sterane rise occurring against persistent hopane abundance;*
2. *the carbon-number window, metal preferences and structural classes of the* 1.1 Ga *geoporphyrin record;*
3. *the independent paleoredox proxy constraints that define the three oxygen windows.*

*The underlying lattice, the $C_{2h}$ symmetry of each core, and the chiral step-defect remain invariant (Theorem 12).*

*Proof.* Immediate from Propositions 14–18 together with the invariance result of Theorem 12. □

**Remark 4.** *Theorem 19 asserts geometric sufficiency, not exclusivity. Additional ecological or diagenetic factors may modulate absolute abundances; the dual-chrysene volume is nevertheless sufficient to produce the qualitative stratigraphic pattern once the Identification Hypothesis is granted.*

### 4.5 Consistency with the Observed Concentration Pattern

**Proposition 20** (Addition rather than Replacement)**.** *The model predicts that the late-Tonian increase in $S/H$ is driven primarily by the addition and quantitative expansion of the sterane (State* M*) signal rather than by a wholesale decline in hopane abundance. This prediction is consistent with the empirical record summarized in Proposition 2.*

The prediction that hopane inventories remain substantial is directly testable against absolute concentration measurements (ng $g^{-1}$ TOC) as further contamination-controlled data sets become available.

## 5 Algebraic Framework for Dual-Catalyst Transformations

The geometric constructions of Section 3 are now lifted into an algebraic setting that makes the admissible transformations, their dependence on the external redox parameter, and the resulting concentration dynamics amenable to formal inference. All structures remain images under the Identification Hypothesis map $\Phi : I_C \to \mathcal{M}$.

### 5.1 Chrysene Platform and Substitution Classes

**Definition 12** (Chrysene Platform)**.** *Let $C$ denote the unsubstituted chrysene skeleton of native $C_{2h}$ symmetry. A* substituted chrysene *is an element of the free module generated by $C$ over the ring of formal substitution labels.*

**Definition 13** (Substitution Classes)**.** *Two principal substitution classes are distinguished:*

$$\mathcal{H} = \mathrm{span}\{C_{6,12},\ C_{3,6,12},\ C_{3,6,9,12}\},$$
$$\mathcal{S} = \mathrm{span}\{C_{2,5,8,11}\}.$$

*Elements of $\mathcal{H}$ are called Family-H geometries; elements of $\mathcal{S}$ are called Family-S geometries. The full catalyst space is the direct sum*

$$\mathcal{V} = \mathcal{H} \oplus \mathcal{S}.$$

**Definition 14** (Dual-Volume Configuration)**.** *A* dual-volume configuration *is an ordered pair*

$$\gamma = (\sigma_{\mathrm{sub}},\ \kappa_{\mathrm{cat}}) \in \mathcal{V} \times \mathcal{V},$$

*where $\sigma_{\mathrm{sub}}$ occupies the substrate position and $\kappa_{\mathrm{cat}}$ occupies the catalyst position of the dual-chrysene reactive volume.*

## 5.2 Transformation Operators

**Definition 15** (Fundamental Operators)**.** *The following continuous families of operators act on dual-volume configurations and on the resulting molecular species. All operators are parameterized by the external redox coordinate $\rho \in [0, 1]$.*

1. ***Substrate transformation***

$$\mathcal{T}_{\mathrm{sub}}(\rho) : \sigma_{\mathrm{sub}} \longmapsto \textit{nucleobase pair}.$$

*This operator is essentially independent of $\rho$ under the anaerobic competence of the patent description and remains available at all subsequent values of $\rho$.*

2. ***Membrane-embedding operator (Family H)***

$$\mathcal{T}^{\mathrm{H}}_{\mathrm{mem}}(\rho) : \kappa_{\mathrm{cat}} \in \mathcal{H} \longmapsto \textit{membrane-embedded hopanoid}.$$

*The operator is constitutively active; its image lies in the membrane lipid fraction for every $\rho$.*

3. ***Silencing operator (Family S)***

$$\mathcal{T}_{\Sigma}(\rho) : \kappa_{\mathrm{cat}} \in \mathcal{S} \longmapsto \textit{gene-intercalated silencing complex}.$$

*Its efficacy is modulated by the function $\sigma(\rho)$ of Definition 6.*

4. ***Membrane-sterol operator (Family S)***

$$\mathcal{T}_{\mathrm{M}}(\rho) : \kappa_{\mathrm{cat}} \in \mathcal{S} \longmapsto \textit{cholesterol-like membrane component}$$

*Its activity increases with $c_S(\rho)$.*

5. ***Functional transition operator***

$$\mathcal{T}_{\Sigma\to\mathrm{M}}(\rho) = \mathcal{T}_{\mathrm{M}}(\rho) \circ \mathcal{T}_{\Sigma}(\rho)^{-1}$$

*(defined on the support where $\sigma(\rho) > 0$). This operator realizes the continuous passage from State $\Sigma$ to State $\mathrm{M}$ and induces the membrane–gene mapping $\Phi_{\Sigma\to\mathrm{M}}$ of Definition 8.*

**Definition 16** (Exogenous-to-Endogenous Operator)**.** *Let $\mathcal{E}(\rho)$ be the operator that replaces an exogenous supply of a geometry $\kappa \in \mathcal{V}$ by the corresponding endogenous biosynthetic pathway (squalene-cyclase / oxidosqualene-cyclase superfamily). $\mathcal{E}(\rho)$ is the identity at $\rho = 0$ (purely exogenous regime) and becomes the dominant supply map for large $\rho$.*

## 5.3 State Space and Concentration Dynamics

**Definition 17** (State Space)**.** *The instantaneous state of the dual-catalyst system is an element*

$$\xi(\rho) = \big(\mu_{\mathrm{H}}(\rho),\ c_S(\rho),\ \sigma(\rho),\ \alpha_{\mathrm{M}}(\rho)\big) \in [0, 1]^4,$$

*where*

- *$\mu_{\mathrm{H}}(\rho)$ is the occupancy of Family-H geometries,*
- *$c_S(\rho)$ is the concentration of Family-S geometries,*
- *$\sigma(\rho)$ is the residual silencing efficacy,*
- *$\alpha_{\mathrm{M}}(\rho)$ is the fraction of Family S that has undergone the transition $\Sigma \to \mathrm{M}$.*

**Proposition 21** (Admissible Trajectories)**.** *Any continuous trajectory $\xi(\rho)$ compatible with the operators of Definition 15 must satisfy:*

1. *$\mu_{\mathrm{H}}(\rho)$ is non-increasing and bounded away from zero (constitutive membrane embedding of Family H);*
2. *$c_S(\rho)$ is non-decreasing;*
3. *$\sigma(\rho)$ is non-increasing with $\sigma(0) = 1$ and $\sigma(1) = 0$;*
4. *$\alpha_{\mathrm{M}}(\rho)$ is non-decreasing. For quantitative illustration we adopt the constitutive leading-order relation*

$$\alpha_{\mathrm{M}}(\rho) \ \propto\ c_S(\rho)\big(1 - \sigma(\rho)\big)$$

*as a modeling choice compatible with the operators. Any other monotonic map that respects the same boundary conditions may be substituted without affecting the qualitative theorems of this section.*

*Proof.* Items (1)–(3) are immediate from the monotonicity properties built into $\mathcal{T}^{\mathrm{H}}_{\mathrm{mem}}$, $c_S(\rho)$ and $\sigma(\rho)$. Item (4) follows because the image of $\mathcal{T}_{\Sigma\to\mathrm{M}}(\rho)$ is populated only to the extent that Family-S material is available and is no longer held in the silencing state. □

**Theorem 22** (Concentration Asymptotics)**.** *Under the admissible dynamics of Proposition 21 one has the asymptotic relations*

$$\lim_{\rho\to 0} \mu_{\mathrm{H}}(\rho) = \mu_{\mathrm{H}}^{\max}, \qquad \lim_{\rho\to 0} c_S(\rho) = c_S^{\min} \ll 1,$$

$$\lim_{\rho\to 1} \mu_{\mathrm{H}}(\rho) \geq \mu_{\mathrm{H}}^{\infty} > 0, \qquad \lim_{\rho\to 1} \alpha_{\mathrm{M}}(\rho) = 1.$$

*Consequently the hopanoid inventory remains substantial at all $\rho$, while the sterane (State-M) inventory becomes dominant only after the silencing activity $\sigma(\rho)c_S(\rho)$ has collapsed.*

*Proof.* Direct integration of the monotonicity constraints in Proposition 21 together with the boundary values of $\sigma$ and $c_S$. □

### 5.4 Invariance and Commutativity

**Theorem 23** (Commutativity with the Geometric Core)**.** *The transformation operators of Definition 15 commute with the action of the structure-preserving map $\Phi$ on the underlying lattice, the $C_{2h}$ symmetry, and the chiral step-defect. In particular, every operator leaves the geometric core invariant.*

*Proof.* Each operator acts on substitution labels and on functional state, never on the combinatorial graph of the chrysene skeleton itself. The claim follows from the factorization of $\Phi$ through that graph (cf. Theorem 12). □

**Corollary 2** (Persistence of Stereochemical Information)**.** *The chiral step-defect is transported unchanged by every operator $\mathcal{T}_{\text{sub}}$, $\mathcal{T}^{\text{H}}_{\text{mem}}$, $\mathcal{T}_{\Sigma}$, $\mathcal{T}_{\text{M}}$ and $\mathcal{T}_{\Sigma\to\text{M}}$.*

### 5.5 Summary of the Algebraic Apparatus

The set $\{\mathcal{T}_{\text{sub}}, \mathcal{T}^{\text{H}}_{\text{mem}}, \mathcal{T}_{\Sigma}, \mathcal{T}_{\text{M}}, \mathcal{T}_{\Sigma\to\text{M}}, \mathcal{E}\}$ together with the state space $\xi(\rho)$ constitutes a complete algebraic calculus for the dual-catalyst system. All qualitative inferences drawn in Sections 3 and 4—co-existence, constitutive hopanoid embedding, redox-controlled silencing-to-membrane transition, membrane–gene mapping, persistence of hopanes, and late rise of steranes—are recovered as formal consequences of the monotonicity and boundary properties of these operators. Quantitative concentration trajectories may now be obtained by specifying explicit functional forms for $\sigma(\rho)$ and $c_S(\rho)$ and integrating the resulting ordinary differential equations on the state space $\xi(\rho)$.

The algebraic constraints of Proposition 21 and Theorem 22 determine the admissible evolution of the state vector $\xi(\rho)$. Figure 1 displays one explicit trajectory generated by functional forms that obey every monotonicity and boundary condition of the framework. Family-H occupancy remains high at both ends of the redox interval, the silencing activity $\sigma(\rho)c_S(\rho)$ collapses through Window 2, and the sterane signal (proportional to $\alpha_M(\rho)c_S(\rho)$) rises only after that collapse. The same panel therefore recovers, as a direct numerical consequence of the operators, the two central empirical regularities of the hopane–sterane record: persistent hopane abundance and a delayed sterane rise.

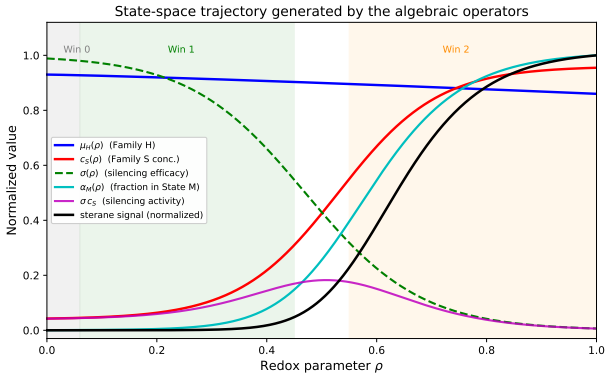


**Figure 1:** State-space trajectory generated by the algebraic operators of Section 5. Blue: Family-H occupancy $\mu_H(\rho)$. Red: Family-S concentration $c_S(\rho)$. Green dashed: silencing efficacy $\sigma(\rho)$. Cyan: fraction $\alpha_M(\rho)$ that has undergone the $\Sigma \to$ M transition. Magenta: instantaneous silencing activity $\sigma(\rho)c_S(\rho)$. Black: normalized sterane signal. Shaded regions indicate the three oxygen windows. The trajectory satisfies all admissibility conditions of Proposition 21 and realizes the asymptotic relations of Theorem 22.

## 6 Testable Predictions and Open Questions

The geometric model generates a finite set of empirical consequences that can be confronted with existing or near-term analytical data. Each prediction is independent of the interpretive narrative and may be tested directly. Open problems that limit present resolution are recorded simultaneously.

### 6.1 Predictions

**Prediction 1** (Residual Signatures of State $\Sigma$)**.** *Mid-Proterozoic bitumen and kerogen are predicted to retain low-concentration molecular or regiochemical signatures attributable to the silencing form (State $\Sigma$) of Family S. These signatures should be distinct from the mature sterane assemblages of Window 2 and may appear as unusual substitution patterns, partially rearranged intermediates, or anomalous carbon-number distributions within the $C_{26}$–$C_{30}$ range.*

**Prediction 2** (Timing of Endogenous Capture versus Sterane Rise)**.** *The first appearance of endogenous sterol-biosynthetic genes (oxidosqualene cyclase and associated tailoring enzymes) is predicted to precede, or at most coincide with, the late-Tonian rise of regular steranes. A measurable stratigraphic offset in which the genes are present while the sterane signal remains weak would be consistent with a continuing regulatory (State $\Sigma$) role prior to full*

*conversion to State* M.

**Prediction 3** (Co-variation with Paleoredox Proxies)**.** *Once the* $\Sigma \to \mathrm{M}$ *transition begins, the abundance of regular steranes (and the ratio* $S/H$*) is predicted to co-vary positively with independent local and global oxygen proxies (Cr isotopes, Mo–U enrichment, Fe speciation, etc.). The co-variation should be weaker or absent in Window 1, where Family S remains primarily regulatory.*

**Prediction 4** (Persistence of Hopanes)**.** *Absolute or relative hopane abundances are predicted to remain substantial across the late-Tonian sterane rise. A wholesale collapse of the hopane signal coincident with the sterane increase would falsify the constitutive membrane-embedding of Family H.*

**Prediction 5** (Traces of Membrane–Gene Coupling)**.** *If the membrane–gene mapping of Definition 8 leaves a detectable geometric or isotopic imprint, it may appear as correlated anomalies between sterane carbon-number distributions and nitrogen-isotope or hydrogen-isotope patterns in co-occurring kerogen-bound aromatics of late Window 1 to early Window 2 age.*

## 6.2 Falsifiability

The model would be seriously challenged by any of the following empirical outcomes:

1. Clear evidence that absolute hopane abundances collapse coincident with the late-Tonian sterane rise (contradicting constitutive membrane embedding of Family H).
2. Demonstration that the $2,5,8,11$-substituted geometry lacks intercalation competence under anaerobic conditions (undermining the geometric basis of State $\Sigma$).
3. Discovery of abundant regular steranes in rigorously contamination-controlled mid-Proterozoic successions that remain hopane-dominated in all other respects (contradicting the low-$c_S(\rho)$ prediction for Window 1).
4. Absence of any temporal relationship between independent oxygen proxies and the sterane rise once the $\Sigma \to \mathrm{M}$ transition is expected to begin.

These criteria are independent of the interpretive narrative and can be evaluated directly against existing or near-term data.

## 6.3 Open Problems

1. A first-principles kinetic model of the relative rates of Family-H membrane embedding versus Family-S silencing and $\Sigma \to \mathrm{M}$ conversion under explicit early-Earth temperature, pressure and oxygen fugacity has not yet been constructed. Such a model is required to convert the qualitative functional-differentiation argument into quantitative stratigraphic predictions.
2. Current analytical methods recover bulk aromaticity and standard sterane/hopane ratios but do not yet resolve the low-concentration, possibly non-standard substitution patterns expected for residual State-$\Sigma$ molecules in mid-Proterozoic material.
3. The atomistic trajectories of intercalation of the $2,5,8,11$-substituted geometry into nascent nucleic-acid frameworks, and the subsequent release upon rising $\rho$, remain beyond present geometric resolution and define a target for future computational work.
4. Direct experimental demonstration of redox-dependent attenuation of silencing efficacy for a sterane-family chrysene derivative has not been performed; the patent supplies only the structural correspondence, not a measured dose–response curve.
5. The precise geometric mechanism by which the $\Sigma \to \mathrm{M}$ transition maps membrane components onto previously intercalated gene loci is stated formally but has not been reduced to an explicit combinatorial or topological construction inside $I_C$.

**Remark 5.** *The open problems delimit the experimental and computational frontier; they do not weaken the consistencies already established in Section 4. The principal empirical regularities of the hopane/sterane record (persistent hopanes, late-Tonian sterane rise), the geoporphyrin archive, and the independent paleoredox proxies already lie inside the geometric envelopes fixed by the redox-controlled co-existence and functional differentiation of the two catalyst families.*

# 7 Conclusion

**Theorem 24** (Geometric Resolution of the Hopane–Sterane Record)**.** *Under the Identification Hypothesis the dual-chrysene reactive volume of U.S. Patent 12,195,423 supplies both Family H and Family S geometries under the anaerobic conditions of Window 0. Family H is constitutively processed into membrane-embedded hopanoids. Family S begins at low concentration in a gene-silencing state (State* $\Sigma$*), its intercalation competence geometrically supported by the structural correspondence recorded in the patent between the sterane-family substitution pattern and nucleobase-pairing loci. As the redox parameter* $\rho$ *rises,*

*silencing efficacy $\sigma(\rho)$ declines, the concentration $c_S(\rho)$ of Family S increases, and the geometry undergoes a continuous transition into a cholesterol-like membrane component (State* M*). This transition maps the membrane onto the gene loci previously occupied by intercalation permits a formal geometric correspondence that may be read as a signalling channe. Full release from silencing permits cellular replication and the quantitative expansion of the membrane-bound sterane population with eukaryotic abundance. Both families begin as exogenous products of the metamaterial and are later captured by endogenous biosynthetic pathways. The mid-Proterozoic hopane dominance and the late-Tonian sterane rise, occurring against a background of persistent hopane abundance, are the geological expression of this redox-controlled functional differentiation. The underlying lattice, the $C_{2h}$ symmetry of each core, and the chiral step-defect remain invariant throughout.*

*Proof.* The dual-chrysene volume co-projects a nucleobase pair from the substrate core and catalyst geometries from the catalyst core (Definition 2). Both families are present at $\rho = 0$ (Definition 3). Family H is rapidly membrane-embedded (Proposition 8). Family S occupies State $\Sigma$ with intercalation competence supplied by the patent correspondence (Definitions 4 and 5). The functions $\sigma(\rho)$ and $c_S(\rho)$ govern the progressive release from silencing and the rise of State M (Definitions 6, 7 and Proposition 9). The $\Sigma \to$ M transition realizes the membrane–gene mapping (Definition 8). Full release permits replication and quantitative expansion of the sterane signal (Definition 9). The geometric core itself is independent of $\rho$ (Theorem 12). Confrontation with the hopane/sterane, geoporphyrin and paleoredox records recovers the observed stratigraphic pattern as the image of this functional differentiation (Theorem 19 and Proposition 20). □

The same geometric object therefore accounts for constitutive hopanoid membranes, redox-controlled silencing and membrane–gene coupling of Family S, and the observed pattern of persistent hopanes plus rising steranes. The subsequent evolutionary capture of these geometries by endogenous gene sets eliminates dependence on external supply of the substituted chrysene cores while preserving the functional distinction between the two families in the modern biosphere. The metamaterial therefore remains continuous from the anaerobic baseline of Window 0, through the progressive oxygenation of the Proterozoic, to the oxygenated atmosphere and eukaryotic membranes of the present day.

# A Literature Review of Paleoredox Proxies and Oxygen-Level Estimates

The three atmospheric oxygen windows employed in the main text are fixed by independent geochemical proxies. The present appendix records the principal observational constraints without theoretical interpretation.

## A.1 Pre-GOE (Window 0): Essentially Anoxic Atmosphere

The strongest constraint on Archean atmospheric composition is the presence of mass-independent fractionation of sulfur isotopes (S-MIF) in sedimentary sulfides and sulfates. Theoretical and experimental work indicates that S-MIF is generated and preserved only when atmospheric $pO_2$ lies below approximately $10^{-5}$ PAL [PK02, ZCC06]. The near-ubiquitous occurrence of large S-MIF signals in rocks older than $\sim 2.45$ Ga therefore establishes that the atmosphere remained essentially anoxic ($pO_2 < 10^{-5}$ PAL) throughout most of the Archean [FBT00, Hol06, LRP14]. Transient "whiffs" of oxygen are recorded in some Neoarchean sections, but these do not erase the long-term S-MIF signal and do not alter the classification of Window 0 as anaerobic for the purposes of the geometric model.

## A.2 The Great Oxidation Event and Early Paleoproterozoic

The irreversible disappearance of S-MIF marks the permanent rise of atmospheric oxygen above the $\sim 10^{-5}$ PAL threshold. High-resolution stratigraphic studies place this transition between approximately 2.46 and 2.32 Ga, with the most tightly constrained estimates clustering near 2.33 Ga [BHW+04, LOB+16, GCB+17, PBC+21]. Post-GOE oxygen levels are less precisely known. Lower bounds are set by the loss of S-MIF and the appearance of terrestrial red beds and sulfate evaporites; upper bounds are supplied by the persistence of anoxic deep oceans and by redox-sensitive metal isotopes. Current estimates for the immediate post-GOE atmosphere typically fall in the range $10^{-3}$–$10^{-1}$ PAL, with many mid-range reconstructions favoring values near 0.01–0.02 PAL during the subsequent mid-Proterozoic [LRP14, CRW+16, PRW+14].

## A.3 Mid-Proterozoic ("Boring Billion") Oxygen Levels

From roughly 1.8 to 0.8 Ga atmospheric oxygen appears to have remained low and relatively stable. Chromium-isotope systematics, cerium anomalies, and zinc/iron ratios in marine carbonates consistently indicate $pO_2$ values of approximately 0.1–2 % PAL throughout most of this interval [PRW+14, CRW+16, LKK+16, RPR+13]. Higher estimates (up to $\sim 10$ % PAL) appear in some older literature, but more

recent proxy compilations converge on the lower end of the range. This persistently low-oxygen state corresponds to Window 1 of the main text.

### A.4 Neoproterozoic Oxygenation Event and the Rise to Modern Levels

A second major increase in atmospheric and oceanic oxygen occurred during the Neoproterozoic (approximately 0.85–0.54 Ga). Evidence includes elevated molybdenum and uranium enrichments in black shales, increased sulfate concentrations, iron-speciation records of deep-ocean oxygenation, and the appearance of macroscopic multicellular organisms [CPN07, OSZ12, SWM+15, LRP14]. Quantitative estimates of the magnitude of the rise remain debated; some reconstructions suggest oscillations between ∼ 1 % and ∼ 50 % PAL, while others indicate a more progressive approach toward modern levels (∼ 21 % absolute) by the early Phanerozoic [KMM+22, TM20]. For the geometric model it is sufficient that Window 2 records a sustained secular increase from the low mid-Proterozoic baseline toward modern atmospheric composition.

#### Summary of Adopted Ranges

The three windows used in the main text are therefore anchored as follows:

| Window | Approximate age | Adopted $pO_2$ range |
|---|---|---|
| 0 | > 2.4 Ga | $< 10^{-5}$ PAL (anaerobic) |
| 1 | ∼ 2.3–0.8 Ga | ∼ 0.1–2 % PAL |
| 2 | < 0.85 Ga | rising toward ∼ 1 PAL |

These ranges are conventional working intervals consistent with the bulk of the current proxy literature; they are not claimed to be unique or definitive. The geometric constructions of the main text depend only on the existence of three qualitatively distinct successive regimes, not on the precise numerical bounds.

## B Background on the Chrysene Formalism and Related Work

The present paper belongs to a systematic program that treats the origin, continuity and functional differentiation of the biosphere as the image of a single geometric object—the dual-chrysene reactive volume—under a structure-preserving map from a pure-mathematical manifold to molecular reality. The program is known collectively as the Chrysene Formalism.

### B.1 Foundational Sources

The empirical starting point is the encoded, integrated synthesis of nucleic acids and phospholipids from substituted chrysene cores under anaerobic conditions, demonstrated in U.S. Patent 12,195,423 [Sch25]. The patent establishes that a dual-chrysene configuration can co-project an informational cipher (nucleobase pair) and a membrane component from a single geometric unit, and it records a structural correspondence between the sterane-family substitution pattern and nucleobase-pairing loci—the geometric warrant for the intercalation competence employed in the main text.

The pure-mathematical substrate of the Formalism is developed in three complementary monographs. The cohomological and operator-algebraic foundations appear in [Sch26b]; the tensorial and maximal-entropy formulation is given in [Sch26g]; and the geometric continuity of the biosphere from the dual-chrysene volume is set out in [Sch26h]. Together these works supply the Identification Hypothesis (the structure-preserving map $\Phi : I_C \to \mathcal{M}$) that is assumed throughout the present article.

### B.2 Empirical and Geometric Sequence in the Annals

A series of papers in the *Annals of the Chrysene Formalism* has converted the abstract geometric claims into concrete consistency tests against the public molecular-fossil and geochemical records:

- The universal blueprint and the single-metamaterial hypothesis are stated in [Sch26i] and [Sch26f].
- Differential catalyst geometries of the dual-chrysene volume, the hopanoid–sterane asymmetry, and the transition from environmental to endogenous supply are examined in [Sch26a].
- Kerogen is interpreted as a macromolecular geometric archive of the same lattice in [Sch26d].
- The dual-chrysene cage rearrangement that conserves an 18 $\pi$-electron aromatic pathway and accounts for the 1.1 Ga geoporphyrin record is derived in [Sch26c].
- The persistent chiral step-defect of the chrysene lattice is shown to be consistent with the homochirality of amino acids, sugars and membrane lipids, and with the meteoritic record, in [Sch26e].

The present work extends that sequence by equipping the dual-chrysene volume with a continuous redox parameter and with two functional states for the sterol-directed family. It thereby converts the hopane–sterane stratigraphic pattern from an empirical asymmetry into a geometric consequence of co-existence, gene silencing, membrane–gene coupling, and redox-controlled functional differentiation.

### B.3 Relation to the Broader Origin-of-Life Literature

Classical origin-of-life research has largely treated the emergence of informational polymers, membrane compartmentalization, and metabolic networks as separate problems, often solved by distinct chemical scenarios. The Chrysene Formalism inverts this order of explanation: a single, persistent geometric object is shown to be competent, under the anaerobic conditions of the patent, for the simultaneous production of a nucleobase pair and a membrane component, and the subsequent evolutionary and redox history of the biosphere is read as the functional differentiation and endogenous capture of that same object. The series of Annals papers cited above constitutes the first systematic attempt to test this inversion against the contamination-controlled molecular-fossil record, the kerogen archive, the geoporphyrin record, and independent paleoredox proxies.

The mathematical apparatus introduced in Section 5 of the present paper—substitution classes, transformation operators, and the state space $\xi(\rho)$—is intended to make the admissible trajectories of this differentiation formally transparent and quantitatively predictive, thereby linking the geometric claims of the Formalism to concrete concentration dynamics that can be confronted with future analytical data.

## References


[BHW+04] A. Bekker, H. D. Holland, P.-L. Wang, III Rumble, D., H. J. Stein, J. L. Hannah, L. L. Coetzee, and N. J. Beukes. Dating the rise of atmospheric oxygen. *Nature*, 427:117–120, 2004.

[CPN07] D. E. Canfield, S. W. Poulton, and G. M. Narbonne. Late-neoproterozoic deep-ocean oxygenation and the rise of animal life. *Science*, 315:92–95, 2007.

[CRW+16] D. B. Cole, C. T. Reinhard, X. Wang, B. Gueguen, G. P. Halverson, T. Lyons, and N. J. Planavsky. A shale-hosted Cr isotope record of low atmospheric oxygen during the Proterozoic. *Geology*, 44:555–558, 2016.

[FBT00] J. Farquhar, H. Bao, and M. Thiemens. Atmospheric influence of Earth's earliest sulfur cycle. *Science*, 289:756–758, 2000.

[GCB+17] A. P. Gumsley, K. R. Chamberlain, W. Bleeker, U. Söderlund, M. O. de Kock, E. R. Larsson, and A. Bekker. Timing and tempo of the Great Oxidation Event. *Proceedings of the National Academy of Sciences*, 114:1811–1816, 2017.

[Hol06] H. D. Holland. The oxygenation of the atmosphere and oceans. *Philosophical Transactions of the Royal Society B*, 361:903–915, 2006.

[KMM+22] A. J. Krause, B. J. W. Mills, A. S. Merdith, T. M. Lenton, and S. W. Poulton. Extreme variability in atmospheric oxygen levels in the late Precambrian. *Science Advances*, 8:eabm8191, 2022.

[LKK+16] X.-M. Liu, L. C. Kah, A. H. Knoll, H. Cui, A. J. Kaufman, R. V. Krishnan, and R. M. Hazen. Tracing Earth's $O_2$ evolution using Zn/Fe ratios in marine carbonates. *Geobiology*, 14:1–14, 2016.

[LOB+16] G. Luo, S. Ono, N. J. Beukes, D. T. Wang, S. Xie, and R. E. Summons. Rapid oxygenation of Earth's atmosphere 2.33 billion years ago. *Science Advances*, 2:e1600134, 2016.

[LRP14] T. W. Lyons, C. T. Reinhard, and N. J. Planavsky. The rise of oxygen in Earth's early ocean and atmosphere. *Nature*, 506:307–315, 2014.

[OSZ12] L. M. Och and G. A. Shields-Zhou. The Neoproterozoic oxygenation event: environmental perturbations and biogeochemical cycling. *Earth-Science Reviews*, 110:26–46, 2012.

[PBC+21] S. W. Poulton, A. Bekker, V. M. Cumming, A. L. Zerkle, D. E. Canfield, and D. T. Johnston. A 200-million-year delay in permanent atmospheric oxygenation. *Nature*, 592:232–236, 2021.

[PK02] A. A. Pavlov and J. F. Kasting. Mass-independent fractionation of sulfur isotopes in Archean sediments: strong evidence for an anoxic Archean atmosphere. *Astrobiology*, 2:27–41, 2002.

[PRW+14] N. J. Planavsky, C. T. Reinhard, X. Wang, D. Thomson, P. McGoldrick, R. H. Rainbird, T. Johnson, W. W. Fischer, and T. W. Lyons. Low mid-Proterozoic atmospheric oxygen levels and the delayed rise of animals. *Science*, 346:635–638, 2014.

[RPR+13] C. T. Reinhard, N. J. Planavsky, L. J. Robbins, C. A. Partin, B. C. Gill, S. V. Lalonde, A. Bekker, K. O. Konhauser, and T. W. Lyons. Proterozoic ocean redox and atmospheric oxygenation. *Proceedings of the National Academy of Sciences*, 110:5357–5362, 2013.

[Sch25] Charles D. Schaper. Encoded design integrated synthesis of nucleic acids, and phospholipids, and related pharmaceutical products, 2025. Patent US 12,195,423.

[Sch26a] Charles D. Schaper. Differential catalyst geometries of the dual-chrysene metamaterial: Hopanoid–sterane asymmetry and the transition from environmental to endogenous supply annals of the chrysene formalism. *Annals of the Chrysene Formalism*, 1:196–208, 2026.

[Sch26b] Charles D. Schaper. *Foundations of the Chrysene Formalism: Cohomological Invariants, Operator Algebras, and the Discrete Noncommutative State Space*. Schaper Systems Press, San Francisco, CA, 2026. ISBN: 979-8-950371-08-0.

[Sch26c] Charles D. Schaper. Geometric origin of the photosynthetic macrocycle: Dual-chrysene cage rearrangement, 18 $\pi$-electron conservation, and the 1.1 Ga geoporphyrin record. *Annals of the Chrysene Formalism*, 1:221–234, 2026.

[Sch26d] Charles D. Schaper. Kerogen as a geometric archive of the chrysene formalism: Macromolecular aromatic networks, dimensional signatures, and metal integration in pre-cambrian shales. *Annals of the Chrysene Formalism*, 1:209–220, 2026.

[Sch26e] Charles D. Schaper. Persistent chiral step-defect of the chrysene lattice: Homochirality of amino acids, sugars, and membrane lipids, and consistency with the meteoritic record. *Annals of the Chrysene Formalism*, 1:235–244, 2026.

[Sch26f] Charles D. Schaper. Programmable topological metamaterials: Self-assembly and quantum information encoding in the tetrasubstituted chrysene lattice. *Annals of the Chrysene Formalism*, 1:169–177, 2026.

[Sch26g] Charles D. Schaper. *Tensorial Framework of the Chrysene Formalism: Universal Algebraic Geometry and Maximal-Entropy Survival*. Schaper Systems Press, San Francisco, CA, 2026. ISBN: 979-8-950371-03-5.

[Sch26h] Charles D. Schaper. *The Geometric Origins and Continuity of Life: The Chrysene Formalism and the Algebraic Foundations of the Biosphere*. Schaper Systems Press, San Francisco, CA, 2026. ISBN: 979-8-950371- 02-8.

[Sch26i] Charles D. Schaper. The universal blueprint: One encodable topological metamaterial to explain the origin, intelligence, and evolution of life. *Annals of the Chrysene Formalism*, 1:178–195, 2026.

[SWM+15] E. A. Sperling, C. J. Wolock, A. S. Morgan, B. C. Gill, M. Kunzmann, G. P. Halverson, F. A. Macdonald, A. H. Knoll, and D. T. Johnston. Statistical analysis of iron geochemical data suggests limited late Proterozoic oxygenation. *Nature*, 523:451–454, 2015.

[TM20] R. Tostevin and B. J. W. Mills. Reconciling proxy records and models of Earth's oxygenation during the Neoproterozoic and Palaeozoic. *Interface Focus*, 10:20190137, 2020.

[ZCC06] K. Zahnle, M. Claire, and D. Catling. The loss of mass-independent fractionation in sulfur due to a Palaeoproterozoic collapse of atmospheric methane. *Geobiology*, 4:271–283, 2006.